

## A modified replacement beam for analyzing building structures with damping systems

Hadi Moghadasi Faridani<sup>\*1</sup> and Antonio Capsoni<sup>2a</sup>

<sup>1</sup>*Department of Civil and Environmental Engineering, Politecnico di Milano,  
32 Leonadro da Vinci, Milan, 20133, Italy*

<sup>2</sup>*Department of Architecture, Built Environment and Construction Engineering, Politecnico di Milano,  
32 Leonadro da Vinci, Milan, 20133, Italy*

*(Received May 9, 2015, Revised February 25, 2016, Accepted April 1, 2016)*

**Abstract.** This paper assesses efficiency of the continuum method as the idealized system of building structures. A modified Coupled Two-Beam (CTB) model equipped with classical and non-classical damping has been proposed and solved analytically. In this system, complementary (non-classical) damping models composed of bending and shear mechanisms have been defined. A spatial shear damping model which is non-homogeneously distributed has been adopted in the CTB formulation and used to equivalently model passive dampers, viscous and viscoelastic devices, embedded in building systems. The application of continuum-based models for the dynamic analysis of shear wall systems has been further discussed. A reference example has been numerically analyzed to evaluate the efficiency of the presented CTB, and the optimization problems of the shear damping have been finally ascertained using local and global performance indices. The results reveal the superior performance of non-classical damping models against the classical damping. They show that the critical position of the first modal rotation in the CTB is reliable as the optimum placement of the shear damping. The results also prove the good efficiency of such a continuum model, in addition to its simplicity, for the fast estimation of dynamic responses and damping optimization issues in building systems.

**Keywords:** building structural systems; continuum model; replacement beam (RB); coupled two-beam (CTB); classical damping; non-classical damping; passive damping

### 1. Introduction

The real static or dynamic response of structures is commonly something different from the sum of the responses of the individual elements because structural integrity guarantees that the elements work together in a properly designed system and consequently, the structure develops some global response through the complex interaction of its elements (Zalka 2012). For this reason, a global approach, where the structure is imagined in a unitary fashion, may be of interest. In this case, the key point in structural design becomes selection of a suitable model truly

---

<sup>\*</sup>Corresponding author, Ph.D., E-mail: [hadi.moghadasi@polimi.it](mailto:hadi.moghadasi@polimi.it)

<sup>a</sup>Associate Professor, E-mail: [antonio.capsoni@polimi.it](mailto:antonio.capsoni@polimi.it)

reproducing the actual characteristics of the original structure.

Simple continuum models called Replacement Beams (RB) can be suitable models, as approximately equivalent systems, to capture basic features of dynamic response of regular buildings, especially of tall ones (Smith and Coull 1991, Zalka 2001, Potzta and Kollar 2003). This approach basically consists of the replacement of the complex building (3D) structure by a continuous equivalent (1D) beam. The main advantages of this approximate model compared with the exact analysis methods are to: (1) model the whole structure simply and avoid probable errors in this stage; (2) easily interpret the results because of dealing with less number of data; (3) focus on the most important structural characteristics and ignore those with no essential influence on the structural responses; (4) independently check the correctness of the exact analysis results; (5) preliminarily design the structural systems and determine dimensions of structural members.

Depending on the structural characteristics of building systems, the RB is characterized by a proper kinematical model and equivalent stiffness parameters (Potzta and Kollar 2003, Tarjan and Kollar 2004), which properly represent the real stiffness of the system as a whole. It is however worth noticing that up to now the research works carried out on RBs seldom deal with the full dynamic response including consistent energy dissipation mechanisms.

Given the significant influence of damping on vibration characteristics of building structures, it has been extensively reported in the literature (Keel and Mahmoodi 1986, Mahmoodi *et al.* 1987, Soong and Dargush 1997, Kareem *et al.* 1999, Madsen *et al.* 2003, Marko *et al.* 2004, Trombetti and Silvestri, 2004, 2006, Silvestri and Trombetti 2007, Hwang *et al.* 2006, 2008, Christopoulos and Montgomery 2013).

From the structural engineering point of view, there are a few studies carried out on damping modeling in RBs. The classical damping has been frequently adopted (Tarjan and Kollar 2004, Miranda and Taghvai 2005) in order to model only the base structural damping in the RB formulation. Lavan (2012) has assessed the efficiency of viscous dampers as coupling elements of shear walls to result in viscously coupled shear walls. A shear-type damping has been proposed to model viscous dampers through a continuum approach. Lavan's formulation contains only the flexural stiffness (i.e., an Euler-Bernoulli beam) due to the walls and gives the main structural responses of the viscously coupled walls. The proposed model was based on the fully distribution of identical dampers along the height and no optimization problems were afforded, where non-identical dampers might be placed.

From the mechanical engineering viewpoint, wide investigations on the effects of internal and external, distributed or lumped dissipation sources have been conducted in continuous beams. An exhaustive overview on the most used damping models can be found in the literature (De Silva 2007, Adhikari 2000, Muravskii 2004, Zarubinskaya and Van Horssen 2005, Adhikari and Woodhouse 2001). Conceiving damping properties as a mechanism of vibration reduction or suppression, many studies on the characterization of the vibrational behavior of externally damped beam structures have been proposed throughout the past decades (Kocatürk and Şimşek 2006, Kayacik *et al.* 2008). Also more recently, the effect of the location of damped segments on the vibrations of beams with partially distributed internal viscous damping (DIVD) was investigated (Tsai *et al.* 2009). The vibration equations of a Timoshenko beam with DIVD subjected to transverse loading were derived and the transfer matrix method (TMM) has been used to determine the frequency equations and to study the vibration characteristics. To demonstrate feature of DIVD effects, various damping and restraining conditions have been taken into account. The influence of the damping, length and location of damped segments on the vibration of beams with DIVD has been investigated and discussed. Some researchers (Chen 2011, Capsoni *et al.*

2013, Faridani and Capsoni 2014) extended this latter research with locally distributed Kelvin-Voigt damping. Using a finite element approach by Chen, the quadratic eigenvalue problem of a damped system was formulated to evaluate the eigenfrequencies of the damped Timoshenko beams. The effects of damping amount, lengths and locations of the damped segment, of axial load and of restraint types on the damped natural frequency of beams have been investigated and discussed. Moreover, the investigation of Timoshenko beams and Sandwich beams with DIVD has been generalized referring to a shear slenderness parameter (Capsoni *et al.* 2013). The dependency of DIVD mechanism type is shown on the stiffness characteristics of beams and a general model has been proposed to choose a proper damping mechanism in beams.

However, this study has been devoted to exploit the damping models proposed for damped beams with applications in mechanical engineering and apply them in the RB systems suitable for civil engineering structures. To this end, a more general continuum system (RB) with damping effects, capable of modeling several building structures (e.g., frames, shear wall systems, and wall-frames), has been developed in order to take both the inherent and passive (viscous and viscoelastic) damping into account. The Coupled Two-Beam (CTB) is used, as an efficient RB model, where a bending damping and a shear damping mechanism (Capsoni *et al.* 2013) are adopted for the flexural beam and shear beam as non-classical damping models, respectively. The classical damping has been already considered in the formulation of such a RB. Firstly, the vibration equations of the laterally loaded CTB are derived through Hamilton's principle by taking into account the damping models. A closed-form solution is proposed based on modal analysis for both the damped free vibration analysis and forced vibration analysis.

The present continuous model allows to deal with the presence of local damping devices in a smeared and kinematically coherent way, leading to a compact formulation which conducts simple approaches to the classical optimization problems. A general shear damping pattern is also proposed to take into account the non-uniform distribution of passive damping and suitable locations are suggested for the placement of this damping type based on the degree of coupling of the flexural and shear beams. Equivalent (continuum) properties of discrete passive devices (viscous/viscoelastic) are presented, where differently configured in frameworks. The application of the CTB for modeling the shear wall systems is specifically addressed, where some possible placements of passive dampers are described.

A numerical example of coupled shear walls is investigated using the present RB model. The modal damping ratio resulted by the classical and non-classical damping models are compared, showing that the bending damping is dominantly efficient in comparison with the classical one. The shear damping is used to investigate the optimal characteristics of viscous and viscoelastic dampers through the CTB. Some comparative investigations and sensitivity analyses are conducted using some proper structural indices, resulting in the position of the maximum rotational field as the first estimation of the optimum location of damping. Further investigations are then devoted to evaluate the optimum amount and length of the shear damping.

The results show that the proposed RB system accompanied by the non-classical damping models can be useful and simple tools for the dynamic investigation of building structures. It is also worth noticing that this approach has been primarily conceived as a first step in dealing with structural problems such as approximate dynamic modeling of high-rise and tall buildings, where the (continuous) shear damping density reflects the additional dissipation phenomenon.

## 2. The Coupled Two-Beam (CTB) model

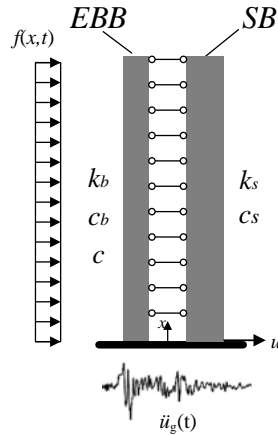


Fig. 1 Damped CTB model composed of a flexural beam and a shear beam

In this section, an idealized model of building systems, the so-called Coupled Two-Beam (CTB), is introduced with a single kinematical field  $u$  (i.e., transversal displacement) and total height of  $L$ . The CTB model (Fig. 1) (Smith and Coull 1991, Miranda and Taghavi 2005) is composed of an Euler-Bernoulli Beam (EBB) and a Shear Beam (SB). The flexural stiffness and shear stiffness of this model can be estimated according to the literature (Potzta and Kollar 2004) or be given from the identification approach (Taghavi and Miranda 2005).

Concerning the dissipation mechanism in the CTB, the classical damping is solely addressed (Miranda and Taghavi 2005). As a main goal of this study, the CTB has been modified by introducing suitable non-classical damping models, in addition to the classical one, in order to take into consideration the inherent damping and passive dissipating phenomena in building structural systems.

Dealing with the steady-state dynamic response of the CTB system, resulted by a harmonic homogeneously distributed external force  $f(x, t) = qe^{i\omega t}$ , a time-independent functional can be introduced. Considering  $q = u$ , the Hamilton's principle is given by

$$\delta \int_{t_0}^{t_1} [L(u, \dot{u}) - R(\dot{u})] dt = \delta \int_{t_0}^{t_1} (T - V + W_f - R) dt = 0 \tag{1}$$

where the Lagrangian  $L$  of the system is determined as the sum of the Total Kinetic Energy  $T$  of the system, the Potential Energy  $V$ , and the work  $W_f$  produced by the external load. The Lagrangian function is given by

$$L(u, \dot{u}) = \frac{1}{2} \int_0^L m(x) (L^2 \dot{u})^2 dx - \frac{1}{2} \int_0^L [k_b(x) u'^2 + k_s(x) (Lu')^2] dx + \int_0^L q(x) u dx \tag{2}$$

and the Rayleigh Dissipation function  $R$  reads

$$R(\dot{u}) = \frac{1}{2} \int_0^L [c(x) (L^2 \dot{u})^2 + c_b(x) (\dot{u}'')^2 + c_s(x) (L^2 \dot{u}')^2] dx \tag{3}$$

Hence, after some manipulations, the time-independent functional can be expressed as

$$H(U) = \frac{1}{2} \int_0^L [k_b(x)u'^2 + i\omega c_b(x)u''^2 + k_s(x)L^2u'^2 + i\omega c_s(x)L^2u'^2 + i\omega c(x)L^4u^2] dx - \int_0^L q(x)u dx - \frac{1}{2} \int_0^L m(x)\omega^2 L^4 u^2 dx \tag{4}$$

Applying the  $L^2$ -norm associated to the above functional in order to minimize the Total Potential Energy, stationarity gives the governing uncoupled equation of the steady-state dynamic response as

$$[k_b(x) + i\omega c_b(x)]u''''(x) - [k_s(x) + i\omega c_s(x)]L^2u''(x) + [m(x)\omega^2 + i\omega c(x)]L^4u(x) = q(x) \tag{5}$$

It should be noted that flexural stiffness  $k_b(x)$ , bending damping  $c_b(x)$ , shear stiffness  $k_s(x)$ , shear damping  $c_s(x)$ , classical damping  $c(x)$ , and mass density  $m(x)$  may be all space-dependent in the formulations depending on the existing mechanical properties in the reference building system.

### 2.1 Damped free vibration analysis

Substituting  $q=0$ ,  $\omega=\omega_j$  and  $u(x)=\phi_j(x)$  into Eq. (5) and assuming constant stiffness, damping, and mass properties, the governing equation of the free vibration analysis is as follows

$$\phi_j''''(x) - \alpha^2\phi_j''(x) - \beta^2\phi_j(x) = 0 \tag{6}$$

where

$$\alpha^2 = \frac{k_s + i\omega_j c_s}{k_b + i\omega_j c_b} L^2 ; \quad \beta^2 = \frac{m\omega_j^2 + i\omega_j c}{k_b + i\omega_j c_b} L^4 \tag{7}$$

Here,  $\phi_j(x)$  is the amplitude of the  $j$  th complex mode shape of vibration and  $\omega_j$  refers to the  $j$  th complex eigenfrequency. A closed-form solution is developed for the CTB, including the damping properties, by imposing the consistent boundary conditions. The general solution of  $\phi_j(x)$  is given by

$$\phi_j(x) = \frac{\sin(\gamma_j x) - (\gamma_j / \lambda_j) \sinh(\lambda_j x) + \eta_j [\cosh(\lambda_j x) - \cos(\gamma_j x)]}{\sin(\gamma_j) - (\gamma_j / \lambda_j) \sinh(\lambda_j) + \eta_j [\cosh(\lambda_j) - \cos(\gamma_j)]} \tag{8}$$

where

$$\lambda_j = \sqrt{\alpha^2 + \gamma_j^2} ; \quad \eta_j = \frac{\gamma_j^2 \sin(\gamma_j) + \gamma_j \lambda_j \sinh(\lambda_j)}{\gamma_j^2 \cos(\gamma_j) + \lambda_j^2 \cosh(\lambda_j)} \tag{9}$$

Note that  $\gamma_j$  is the complex eigenvalue parameter and is obtained by solving the following equation

$$\gamma_j^4 + \alpha^2 \gamma_j^2 - \beta^2 = 0 \tag{10}$$

Since the latter equation is a function of the complex frequencies  $\omega_j$ , an additional equation is required to calculate  $\gamma_j$ . Therefore, using the boundary condition corresponding to zero shear force at the top gives the new equation for computing eigenvalue parameter  $\gamma_j$ , associated with the  $j$  th mode which is a function of the complex parameter  $\alpha^2$ . The governing equation reads

$$2 + \left( 2 + \frac{\alpha^4}{\gamma_j^2 \lambda_j^2} \right) \cos(\gamma_j) \cosh(\lambda_j) = -\frac{\alpha^2}{\gamma_j \lambda_j} \sin(\gamma_j) \sinh(\lambda_j) \quad (11)$$

According to Eq. (10),  $\alpha^2$  can be obtained as the function of  $\gamma_j$  and be substituted into Eq. (11), consequently resulting in an equation to calculate the eigenvalue parameter  $\gamma_j$ . The solution gives two values of  $\gamma_j$  associated with two conjugate eigenmodes. The minimum positive root corresponds to the fundamental eigenproblems, and orderly higher roots help to determine higher modes characteristics.

Because of the dependency of the parameters  $\alpha^2$  and  $\beta^2$  on  $\omega_j$  through Eq. (10), the conjugate eigenfrequencies of each eigenmode is given by

$$\omega_{j1,2} = \frac{-c_2 \pm i\sqrt{4c_1c_3 - c_2^2}}{2c_1} \quad (12)$$

where

$$c_1 = mL^4; \quad c_2 = \gamma_j^2 (c_b \gamma_j^2 + c_s L^2 + cL^4); \quad c_3 = \gamma_j^2 (k_b \gamma_j^2 + k_s L^2) \quad (13)$$

Correspondingly, the damped and free oscillating modes can be directly obtained by substituting the resulted  $\alpha^2$  and  $\gamma_j$  into Eq. (8).

According to Eq. (12), the modal damping ratio associated to each mode is expressed by

$$\zeta_j = -\frac{\operatorname{Re}(\omega_j)}{\sqrt{\operatorname{Re}^2(\omega_j) + \operatorname{Im}^2(\omega_j)}} \quad (14)$$

As mentioned before, the mechanical properties for the damped free vibration analysis were assumed uniform. Concerning non-uniform properties, a FE method can be adapted to solve Eq. (6). When the stiffness and mass properties are uniform, while the damping models are non-uniformly distributed, the following expression is proposed for the estimation of the modal damping ratio

$$\zeta_j = \frac{R_j^{(c)} + R_j^{(c_b)} + R_j^{(c_s)}}{4\pi V_j} = \frac{R_j}{4\pi V_j} \quad (15)$$

where  $R_j^{(c)}$ ,  $R_j^{(c_b)}$ , and  $R_j^{(c_s)}$  are modal Rayleigh Dissipation functions;  $V_j$  is the potential energy associated with the  $j$  th mode;  $R_j$  is the sum of modal Rayleigh functions. Using the modal response  $u_j = \bar{\phi}_j(x)D_j(t)$  in the second term of Eq. (2),  $V_j$  is subsequently defined. Also, the modal Rayleigh function  $R_j$  is obtained by adopting  $u_j$  in Eq. (3). Then, substituting  $R_j$  and  $V_j$  into Eq. (15), after performing some manipulations, the modal damping ratio is given by the following expression

$$\zeta_j = \frac{\frac{L^4}{k_b} \int_0^1 c(x) (\bar{\phi}_j)^2 dx + \frac{1}{k_b} \int_0^1 c_b(x) (\bar{\phi}_j'')^2 dx + \frac{L^2}{k_b} \int_0^1 c_s(x) (\bar{\phi}_j')^2 dx}{2 \int_0^1 \left[ (\bar{\phi}_j'')^2 + \alpha_0^2 (\bar{\phi}_j')^2 \right] dx} \bar{\omega}_j \quad (16)$$

Here,  $\bar{\omega}_j$ ,  $\bar{\phi}_j(x)$ , and  $\alpha_0^2$  are undamped frequency, undamped mode, and non-dimensional stiffness ratio, respectively. Note that  $\alpha_0^2$  can be achieved by omitting the damping coefficients in the definition of  $\alpha^2$  expressed by Eq. (7).

It has been recently demonstrated (Lavan 2012) that a constant shear-type damping can be employed to properly model the uniform distribution of viscous dampers in the structures composed of shear walls. Based on the latter equation, the level of damping caused by the viscous-type dampers can be estimated; hence, the shear damping  $c_s(x)$  in the present CTB is expected to be a more general model to analyze dynamic responses of building structural systems affected by the local distribution of non-identical passive dampers. Considering that the overall modal damping ratio is the summation of the inherent modal damping  $\zeta_{0,j}$  and the additional modal damping  $\zeta_{d,j}$ , the latter one is expressed by

$$\zeta_{d,j} = \frac{\frac{L^2}{k_b} \int_{x_0}^{x_0+L_d} c_s(x) (\bar{\phi}_j')^2 dx}{2 \int_0^1 \left[ (\bar{\phi}_j'')^2 + \alpha_0^2 (\bar{\phi}_j')^2 \right] dx} \bar{\omega}_j \tag{17}$$

where  $c_s(x)$  is distributed in the range  $x_0 \leq x \leq x_0 + L_d$ . For the sake of simplicity,  $c_s(x)$  is assumed to be a linear function in order to practically approximate the distribution of passive damping.

### 2.2 General patterns for shear damping modeling

In order to present a general function for the shear damping, one possibility is to utilize the distribution of undamped modal rotation associated to the fundamental mode. It is expected that a fixed length  $L_d$  around the maximum modal rotation may be the most efficient location for the placement of passive damping. This location may vary, depending on a controlling parameter called degree of coupling  $\alpha_0^2$ . This parameter can be expressed through Eq. (7), where the damping coefficients are neglected. Such a parameter controls the degree of participation of overall flexural and overall shear deformations in the CTB model and thus controls the lateral deflected shape of buildings. A value of  $\alpha_0^2$  equal to zero represents a pure flexural model like an Euler-Bernoulli beam and a value equal to  $\infty$  corresponds to a pure shear model. An intermediate value of  $\alpha_0^2$  corresponds to the case that combines shear and flexural deformations. However, it can be argued that positioning the  $c_s(x)$  around the location of most critical rotation with a compatible pattern with respect to the distribution of rotation may represent a suitable strategy for damped CTB models.

The root of following expression, derived based on the fundamental rotation mode, gives the position of maximum modal rotation along the CTB model

$$\gamma_1^2 \eta_1 \cos(\gamma_1 x) + (\alpha_0^2 + \gamma_1^2) \eta_1 \cosh\left(x\sqrt{\alpha_0^2 + \gamma_1^2}\right) - \gamma_1 \sqrt{\alpha_0^2 + \gamma_1^2} \sinh\left(x\sqrt{\alpha_0^2 + \gamma_1^2}\right) - \gamma_1^2 \sin(\gamma_1 x) = 0 \tag{18}$$

where  $\gamma_1$  and  $\eta_1$  should be obtained from Eqs. (9)-(10) by substituting  $j=1$ .

Consequently, in general, a pentagon-shape model is proposed (Fig. 2(a)) which may be proportionally consistent with the linearized equivalence of the rotation shape at the most critical locations (see Figs. 2(b)-(c)). To introduce this model, a peak shear damping coefficient  $c_{s,max}$  must be chosen and be located at the maximum rotation position. The damping distribution can be then expressed as follows

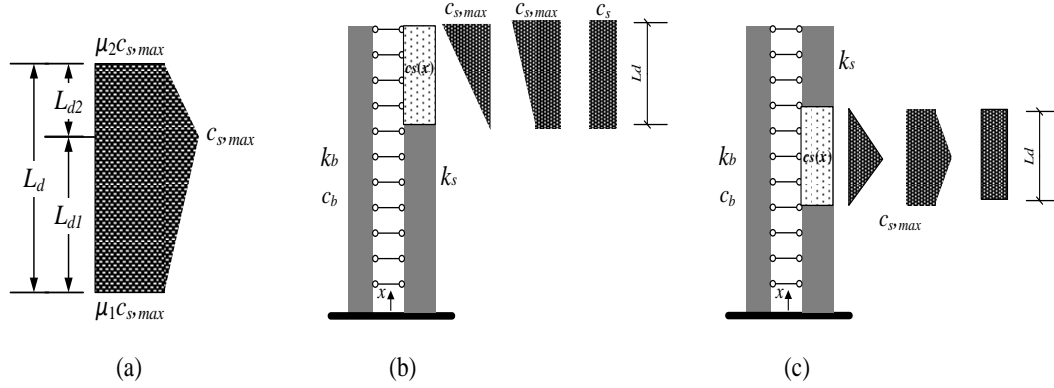


Fig. 2 Non-uniform shear damping model adopted (a) general pattern (b) for CTB with very small  $\alpha_0^2$  (c) for CTB with intermediate  $\alpha_0^2$

$$c_s(x) = \begin{cases} c_{s,\max} \left[ \frac{1-\mu_1}{L_{d1}}(x-x_0) + \mu_1 \right]; & \text{for: } x_0 \leq x \leq x_0 + L_{d1}; 0 \leq \mu_1 \leq 1 \\ c_{s,\max} \left[ \frac{(\mu_2-1)(x-x_0-L_d)}{L_d-L_{d1}} + \mu_2 \right]; & \text{for: } x_0 + L_{d1} \leq x \leq x_0 + L_d; 0 \end{cases} \quad (19)$$

where  $L_{d1}$  is the damped length under the peak rotation elevation. Herein,  $\mu_1$  and  $\mu_2$  may be selected based on the distribution of passive damping along the original building. It should be remarked that a triangular damping shape is achieved when  $\mu_1 = \mu_2 = 0$  and a uniform distribution is resulted with  $\mu_1 = \mu_2 = 1$ .

Fig. 3 shows some viscous-based dampers and relevant configurations which are applicable in frames, coupled shear walls, and wall-frame systems. The equivalent shear damping  $c_s$  and shear stiffness  $k_{s,eq}$  coefficients, corresponding to various passive dampers and structural systems, are presented in Table 1. These coefficients are given by equating the energy dissipation and strain energy of the discrete devices and their continuum equivalences. It is worth noticing that the influence of the additional stiffness  $k_{s,eq}$  due to viscoelastic dampers can be taken into account in the definition of the strain energy in Eq. (17). The dampers vertically installed (Fig. 3) perform based on the relatively vertical velocity created between the left and right members, where transversal loads enforce the system to deflect.

### 2.3 Forced vibration analysis

The response of the non-uniform CTB model subjected to a general force  $f(x,t)$ , accounting for the non-uniform damping mechanisms, is given by the following partial equation of motion

$$m(x) \frac{\partial^2 u(x,t)}{\partial t^2} + c(x) \frac{\partial u(x,t)}{\partial t} + \frac{1}{L^4} \frac{\partial^2}{\partial x^2} \left( c_b(x) \frac{\partial^3 u(x,t)}{\partial t \partial x^2} \right) - \frac{1}{L^2} \frac{\partial}{\partial x} \left( c_s(x) \frac{\partial^2 u(x,t)}{\partial t \partial x} \right) + \frac{1}{L^4} \frac{\partial^2}{\partial x^2} \left( k_b(x) \frac{\partial^2 u(x,t)}{\partial x^2} \right) - \frac{1}{L^2} \frac{\partial}{\partial x} \left( k_s(x) \frac{\partial u(x,t)}{\partial x} \right) = f(x,t) \quad (20)$$

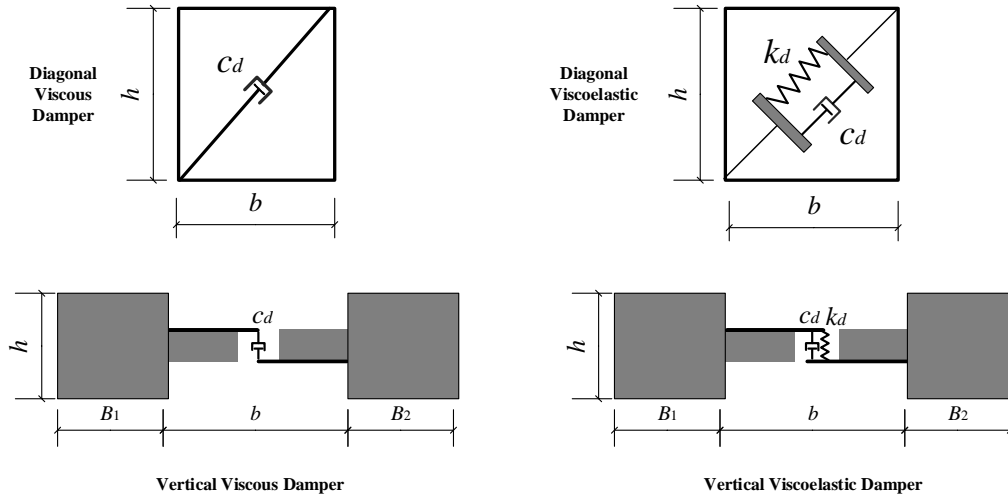


Fig. 3 Various configurations of viscous and viscoelastic dampers in frames and coupled walls

Table 1 Equivalent stiffness and damping coefficients for a single passive damper

Type of dissipative device	Installation direction	Type of structure	Equivalent damping $c_s$	Equivalent stiffness $k_{s,eq}$
viscous damper	diagonal	frame/wall-frame	$\frac{hb^2}{(h^2 + b^2)} c_d^*$	—
		coupled shear walls	$\frac{h(B_1 / 2 + B_2 / 2 + b)^2}{(h^2 + b^2)} c_d$	—
	vertical	coupled shear walls	$\frac{b}{(ht)} \left(1 + \frac{2b}{B_1 + B_2}\right)^2 c_d$	—
viscoelastic damper	diagonal	frame/wall-frame	$\frac{hb^2}{(h^2 + b^2)} c_d^*$	$\frac{hb^2}{(h^2 + b^2)} k_d$
		coupled shear walls	$\frac{h(B_1 / 2 + B_2 / 2 + b)^2}{(h^2 + b^2)} c_d$	$\frac{h(B_1 / 2 + B_2 / 2 + b)^2}{(h^2 + b^2)} k_d$
	vertical	coupled shear walls	$\frac{b}{(ht)} \left(1 + \frac{2b}{B_1 + B_2}\right)^2 c_d$	$\frac{b}{(ht)} \left(1 + \frac{2b}{B_1 + B_2}\right)^2 k_d$

\*  $c_d$ : viscous damping coefficient in dampers

Here, all the mechanical properties (i.e.,  $m$ ,  $c$ ,  $c_b$ ,  $c_s$ ,  $k_b$ , and  $k_s$ ) are previously defined in section 2. The right-hand side of Eq. (20), when the CTB is excited by a horizontal acceleration at the base, should be defined as  $f(x,t) = -m(x)\partial^2 u_g(t) / \partial t^2$ .

Having assumed that the mass and stiffness properties are uniform along the system, a modal analysis approach (Miranda and Taghavi 2005) is employed to calculate the overall responses with superposition of the responses of all the modes of vibrations. Hence, the displacement response  $u(x,t)$  in the CTB model is given by

$$u(x,t) = \sum_{j=1}^n u_j(x,t) = \sum_{j=1}^n \Gamma_j \bar{\phi}_j(x) D_j(t) = \sum_{j=1}^n \frac{\int_0^1 \bar{\phi}_j(x) dx}{\int_0^1 \bar{\phi}_j^2(x) dx} \bar{\phi}_j(x) D_j(t) \quad (21)$$

where  $D_j(t)$  associated to  $j$  th mode can be calculated by solving the following equation

$$\ddot{D}_j(t) + 2\zeta_j \bar{\omega}_j \dot{D}_j(t) + \bar{\omega}_j^2 D_j(t) = \begin{cases} -\ddot{u}_g(t) : \text{Ground Acceleration} \\ f(t)/m_j : \text{Dynamic Force} \end{cases} \quad (22)$$

It should be noted that the contribution of various damping mechanisms to the response must be taken into account through  $D_j(t)$ , using the definition of damping ratio  $\zeta_j$  expressed by Eqs. (14)-(16).

When the non-uniform shear damping is employed to model the passive damping, the modal damping factor in Eq. (22) reads

$$\zeta_j = \zeta_{0,j} + \zeta_{d,j} \quad (23)$$

where the inherent modal damping  $\zeta_{0,j}$  may be calculated using Eq. (16) and the additional damping  $\zeta_{d,j}$  due to the non-homogeneous shear damping is given by Eq. (17).

The inter-story drift ratio,  $IDR(x,t)$ , is an important measure of nonstructural damage and can be evaluated by the derivative of the displacement

$$IDR(x,t) = \frac{\partial u(x,t)}{\partial x} = \frac{1}{L} \sum_{j=1}^n \Gamma_j \bar{\phi}_j'(x) D_j(t) = \frac{1}{L} \sum_{j=1}^n \frac{\int_0^1 \bar{\phi}_j(x) dx}{\int_0^1 \bar{\phi}_j^2(x) dx} \bar{\phi}_j'(x) D_j(t) \quad (24)$$

The absolute acceleration that is a measure of damage to nonstructural acceleration sensitive equipment as well as contents' movement along the floor area

$$\ddot{u}'(x,t) = \ddot{u}_g(t) + \sum_{j=1}^n \Gamma_j \bar{\phi}_j(x) \ddot{D}_j(t) = \ddot{u}_g(t) + \sum_{j=1}^n \frac{\int_0^1 \bar{\phi}_j(x) dx}{\int_0^1 \bar{\phi}_j^2(x) dx} \bar{\phi}_j(x) \ddot{D}_j(t) \quad (25)$$

The time-dependent bending moment  $M(x,t)$  is expressed as

$$M(x,t) = \sum_{j=1}^n M_j(x,t) = \sum_{j=1}^n \Gamma_j \left[ k_b \int_x^1 \bar{\phi}_j''(x) dx - k_s \int_x^1 \bar{\phi}_j(x) dx \right] D_j(t) \quad (26)$$

Also, the shear force  $V(x,t)$  is given by

$$V(x,t) = \sum_{j=1}^n V_j(x,t) = \sum_{j=1}^n \Gamma_j \left[ k_b \int_x^1 \bar{\phi}_j'''(x) dx - k_s \int_x^1 \bar{\phi}_j'(x) dx \right] D_j(t) \quad (27)$$

When the mechanical properties vary along the height (e.g. additional stiffness and damping due to viscoelastic dampers installed in some positions or the variation of stiffness due to absence

of coupling beams), the dynamic characteristics of the continuum model were computed by employing a 1D FE method. For this aim, the CTB model was discretized into elements with the lengths equal to the inter-story height. This FE model can be used also for the analysis of responses where the damping mechanisms are non-uniformly distributed. Some dynamical responses such as vibration energy (D) (Huang and Zhu 2013) and the sum of transfer functions of inter-story drifts (V) (Takewaki 2009), can be also calculated using the FE model.

### 2.4 CTB models for shear wall systems supported by dampers

Amongst load-resisting structural systems of tall buildings, shear walls and coupled shear walls are commonly efficient ones. In addition to high strength and inherent dissipation capability, they are also prone to be properly equipped by passive damping systems for mitigating wind and seismic vibrations. For a single-bay coupled shear wall (see Fig. 4), the equivalent shear stiffness  $k_s$  to be adopted for the CTB can be expressed by

$$k_s = \frac{\ell_b}{h} \left( \frac{\ell_b^2}{12EI_b} + \frac{1}{G\kappa A_b} \right)^{-1} \left( 1 + \frac{B_1 + B_2}{2\ell_b} \right)^2 \tag{28}$$

where  $B_1$  and  $B_2$  are the widths of the left and right shear walls;  $\ell_b$  is connecting beams length;  $h$  is the inter-story height;  $I_b$  and  $\kappa A_b$  are the moment of inertia and shear area of connecting beams;  $E$  and  $G$  are the elastic modulus and shear modulus, respectively. The flexural stiffness  $k_b$  is assumed to be the summation of the flexural stiffness  $EI$  of each single shear wall (i.e.,  $k_b = \sum_{i=1}^N (EI)_i$ ).

The images illustrated in the upper part of Fig. 4 indicate some possible applications of passive dampers, i.e., (S1) diagonal viscous dampers non-homogeneously distributed; (S2) diagonal viscous dampers fully distributed; (S3) diagonal viscoelastic dampers non-homogeneously distributed; (S4) vertical viscoelastic dampers non-homogeneously distributed; (S5) vertical viscoelastic dampers fully distributed, coupling single shear walls or coupled shear walls. Correspondingly, the CTB models with the bending damping  $c_b$  in the flexural beams and the shear damping  $c_s$  as the distributed equivalence of passive dampers are depicted in the lower part of Fig. 4. Also, the CTB model of a wall-frame system supported by viscous dampers is illustrated in Fig. 5. According to the relations presented in Table 1, the suitable shear stiffness and damping, associated with every damping system shown in Figs. 4 and 5, can be used. Note that depending on the amount of damping coefficient  $c_d$  in each damper, the relevant shear damping may be different and correspondingly the shear damping function  $c_s(x)$  may be distributed non-uniformly along the CTB.

## 3. Numerical investigations

### 3.1 Assessment of the CTB model

First of all, the accuracy of proposed solutions for the CTB model is examined with respect to a 13-story RC shear wall (Lavan 2012) retrofitted by identical viscous dampers which are diagonally coupling the walls. The building is excited by the LA07 ground acceleration. The structure corresponds to the case S2 shown in Fig. 4, thus, CTB2 illustrated in Fig. 4 is chosen as the equivalent RB (i.e., the degree of coupling is zero  $\alpha_0^2=0$  and the flexural stiffness solely exists).

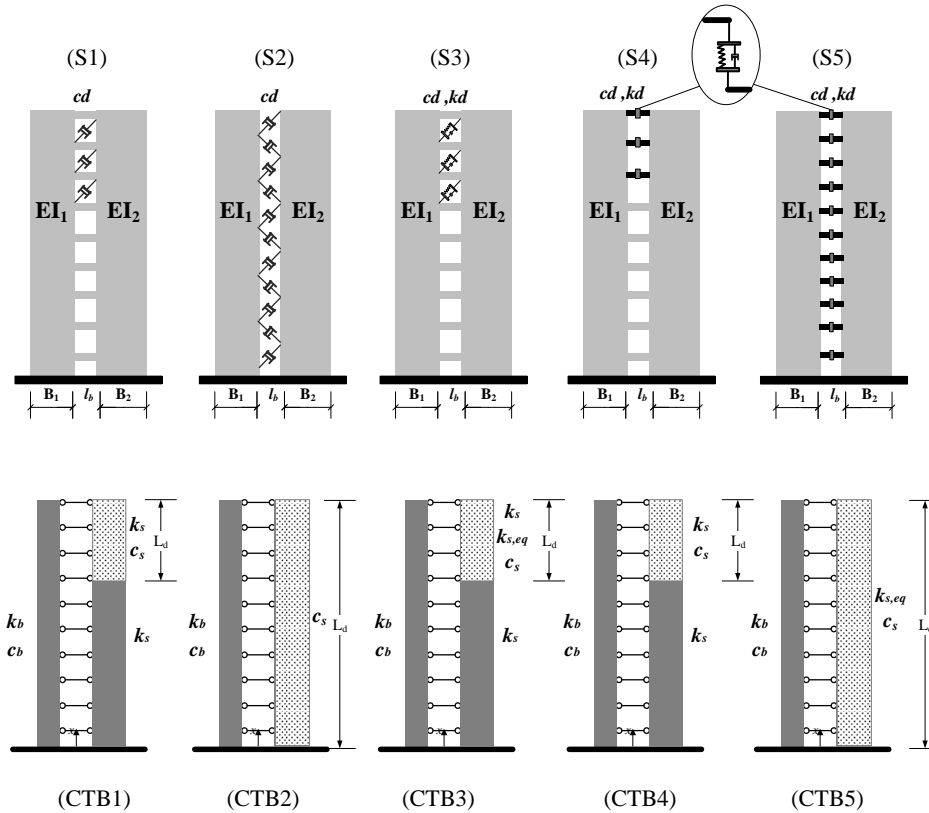


Fig. 4 Shear wall systems equipped with various passive dampers and their equivalent CTB models

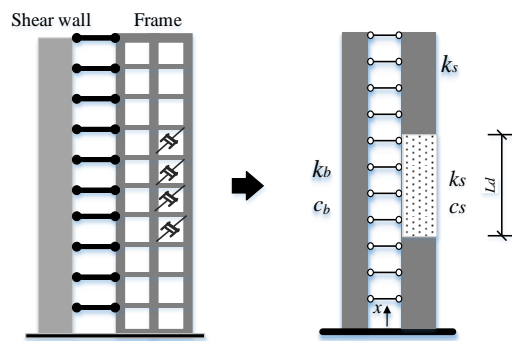


Fig. 5 A wall-frame system equipped with viscous dampers and its equivalent CTB model

Regarding the type and arrangement of dampers, the suitable relation is selected from Table 1 to calculate the equivalent shear damping. Hence, a constant shear damping  $c_s=28000$  kN.s is obtained based on the original damping coefficient of identical dampers. Table 2 gives some of important structural responses presented by Lavan (2012) and those calculated by the present CTB solution. In the analysis, both the inherent damping and additional damping are examined. It should be remarked that the shear damping is solely modelling the passive damping, while the

Table 2 Structural responses by CTB solution and Lavan (2012), obtained for both 5% inherent damping and additional (viscous) damping

Damping sort	5% inherent damping		Passive damping (viscous damper)			
			Discrete approach (Lavan 2012)		Continuous approach	
Response	Lavan (2012)	Present CTB	Time history analysis	Modal spectral analysis	Lavan (2012)	Present CTB
Natural period [s]	3.69	3.69	-	3.76	3.74	3.59
Damping ratio of first mode	0.05	0.05	-	0.265	0.266	0.267
Roof displacement [m]	0.386	0.4	0.165	0.159	0.163	0.176
Max. inter-story drift ratio [%]	1.37	1.35	0.62	0.57	0.58	0.52
Max. absolute acceleration [m/s <sup>2</sup> ]	8.21	7.12	4.38	5.34	5.55	4.53
Total base shear [kN]	9453	9635	5620	4980	5014	6228
Total base moment [kN.m]	230600	238000	126000	112500	113600	114400

bending and classical damping are neglected. The inherent damping is directly considered identical for all the modes. Table 2 indicates that the CTB solutions are reliable against those responses obtained from other methods.

### 3.2 Numerical examples

In this study, a coupled shear wall presented in the literature (Smith and Coull 1991, Takabatake 2010, Bozdogan 2012) is considered (see Fig. 6) and the efficiency of proposed damping mechanisms (i.e., bending and shear damping) is investigated, where the external load uniformly distributed is a harmonic one,  $f(t)=16500\sin(0.9\omega_1t)$ . This force will be updated with respect to the fundamental frequency  $\omega_1$  of the system. A CTB system with equivalent stiffness properties is modeled based on the reference structure. To compare the modal damping ratios calculated using Eqs. (14)-(16), a certain amount of shear damping (i.e.,  $c_s=6\times 10^6$  N.s/m<sup>2</sup>) fully distributed in the reference system is considered. This may be the equivalent (continuous) damping of distributed dampers along the system. Different values of the degree of coupling are obtained by changing the shear stiffness  $k_s$  as the controlling parameter, in order to realize the trend of variation in the damping factor against the degree of coupling. Fig. 7(a) shows this trend using Eqs. (14)-(16) by the first three modes. A very good agreement can be observed from the graphs in Fig. 7(a), showing that Eq. (16) is a reliable definition of the modal damping ratio where a building system is idealized with a CTB model.

The classical damping and bending damping are other energy dissipation mechanisms used in the CTB formulation. To compare the behavior of different damping models, damping ratios associated with the first three modes against the degree of coupling are plotted in Fig. 7(b) and Figs. 8(a)-(b), respectively. Three damping coefficients (i.e., classical, bending, and shear damping) are fixed in such a way that 1% damping ratio be resulted in the fundamental mode. Consequently, the effect of the change in the degree of coupling is identified on the three modal damping factors. It should be remarked that each diagram corresponds to a single damping model solely applied in the analysis. According to Fig. 7(b), the first damping ratio  $\zeta_1$  decreases by the

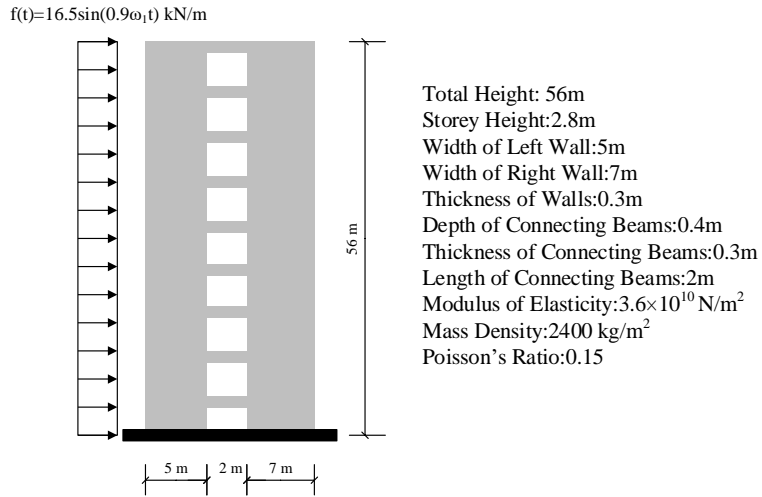


Fig. 6 An asymmetrical coupled shear walls system

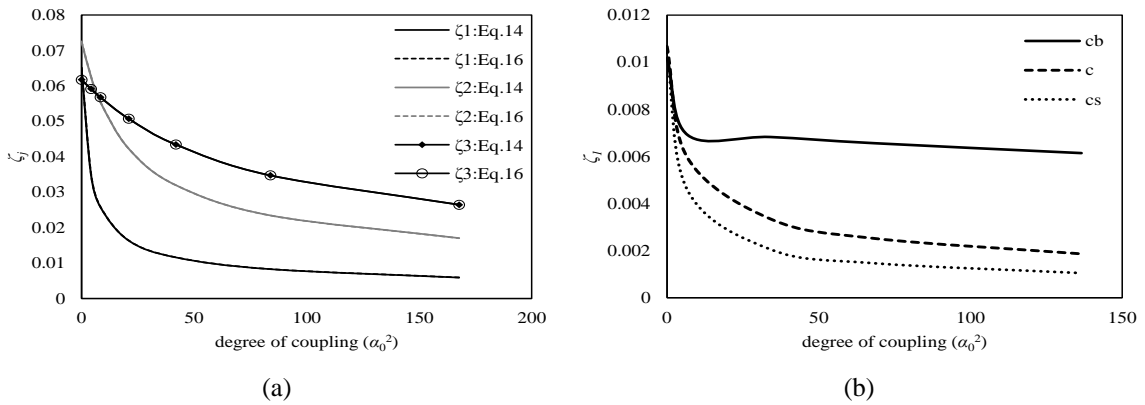


Fig. 7 (a) Comparison of modal damping ratios due to shear damping computed by Eqs. (14)-(16) versus  $\alpha_0^2$  (b) first mode damping ratio against  $\alpha_0^2$  with various damping models

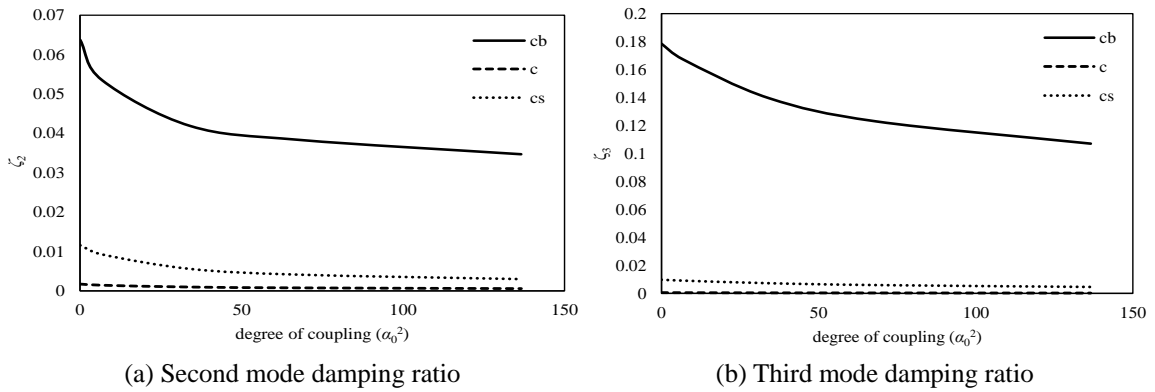


Fig. 8 Modal damping ratios versus  $\alpha_0^2$  obtained from several damping models

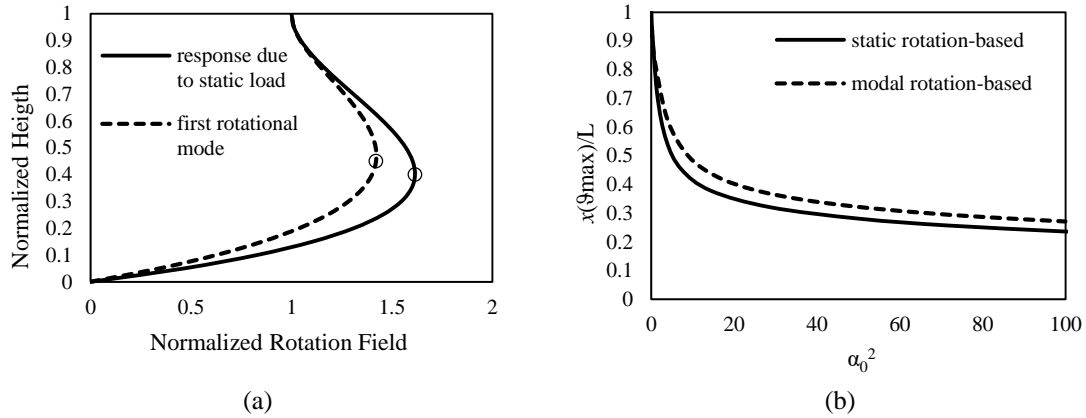


Fig. 9 (a) Distribution of normalized static and modal rotation in coupled walls of the reference structure (b) Trend of position of peak static and modal rotations along the height versus  $\alpha_0^2$

degree of coupling for every damping mechanism, while the diagram associated to the bending damping shows higher values than other two diagrams. It can be seen from Figs. 8(a)-(b) that the modal damping ratios resulted by the classical damping  $c$  are significantly less than those obtained by the bending damping  $c_b$ . This is also observable by comparing the diagrams affected by the shear  $c_s$  and bending  $c_b$  damping. This observation demonstrates that the classical damping in the CTB formulation is incapable of providing identical modal damping ratios, where this assumption is usually assumed in the design.

### 3.2.1 The investigation of damping optimization

First, to ascertain the optimum place of the shear damping, the distribution of rotation induced by the static force and of the first modal rotation along the reference structure is shown in Fig. 9(a). It can be observed that the peak responses of each diagram are identified at the normalized elevations 0.4 and 0.45, respectively, with respect to the base. The distribution of static rotation is obtained under the uniform load. Also, the general position of the maximum static rotation (refer to Eq. (29)) and first modal rotation (refer to Eq. (18)) against the degree of coupling  $\alpha_0^2$  are plotted in Fig. 9(b). Neglecting the time-dependent terms in Eq. (20), where the structure is subjected to a constant static load (i.e., static force due to wind), the root of following equation gives the location of peak static rotation

$$\cosh\left[\alpha_0\left(1-\frac{x}{L}\right)\right] + \alpha_0 \sinh\left(\alpha_0 \frac{x}{L}\right) = 0 \tag{29}$$

Depending on the problem that is subjected to wind or earthquake load, Fig. 9(b) can be applied to initially estimate the suitable location for the placement of shear (passive) damping. Note that the effect of higher modes (i.e., peak rotation position associated to higher modes) is neglected.

Regarding the shear damping model and its possible adaption in the CTB model, the equivalent damping of supplementary dissipating devices in coupled walls (e.g., viscous or viscoelastic dampers) is investigated. For this purpose, the investigation is devoted to controlling dynamic magnification factor (DMF) of tip displacement as a local index and two other global performance indices, which are vibration energy ( $D$ ) and sum of transfer function of inter-story drifts ( $V$ ).

Furthermore, the overall damping factor associated with the fundamental model is considered.

Optimization of Viscous Dampers

Using the shear damping as the additional dissipation mechanism in the CTB, the optimization of its distribution length  $L_d$ , while the inherent damping is set to 5% with a fully distributed bending damping  $c_{b,5\%}$  [N.s/m<sup>2</sup>], is evaluated. The cantilever CTB model of the reference problem is loaded by an external distributed sinusoidal dynamic load,  $f(t)=16500\sin(\omega t)$ , and excitation frequency  $\omega=0.9\omega_1$ , is worth noticing that only the fundamental mode contribution is considered in the response analysis. Concerning a non-uniformly shear damping model with distribution length of  $L_d$ , as presented in Fig. 2(a), considering its maximum amount  $c_{s,max}$  to assign the damping value, two main damping contributions are conceived acted upon by the CTB system and defined as follows

$$\begin{cases} C_b = (c_{b,5\%}) \cdot (A_1 + A_2) L = (c_{b,5\%}) \cdot L \\ C_s = \frac{c_{s,max} (t\ell_b)}{2} [(1 + \mu_1) L_{d1} + (1 + \mu_2) L_{d2}] \end{cases} \Rightarrow \eta = \frac{C_s}{C_b} \quad (30)$$

where  $(A_1+A_2)L=(0.3\times 5+0.3\times 7)\times 56=201.6 \text{ m}^3$  is the equivalent volume of the EBB and  $t\ell_b=0.3\times 2=0.6 \text{ m}^2$  is the equivalent area of the SB cross-section in the CTB. According to Eq. (30), the parameter  $\eta$  is defined as the ratio between the resultant shear (passive) damping  $C_s$  due to the damped segment in the SB and the resultant bending damping  $C_b$  in the EBB, in order to comparatively change the shear damping with respect to the bending one.

The effect of the shape of shear damping is investigated on the CTB response by using a constant length  $L_d=0.2L$ . For the sake of simplicity, two lengths (i.e.,  $L_{d1}, L_{d2}$ ) and controlling coefficients (i.e.,  $\mu_1, \mu_2$ ) to define the damping shapes are assumed identical (see Fig. 2(a)). The DMF of tip displacement is graphed (Fig. 10) versus the maximum damping parameter  $\eta$ , which is associated with the maximum damping coefficient  $c_{s,max}$  located at the position of maximum modal rotation. It can be seen that for  $\eta$  greater than about 0.004 and also for very low values of  $\eta$ , all of the damping shapes show almost a similar influence on the response. The most significant

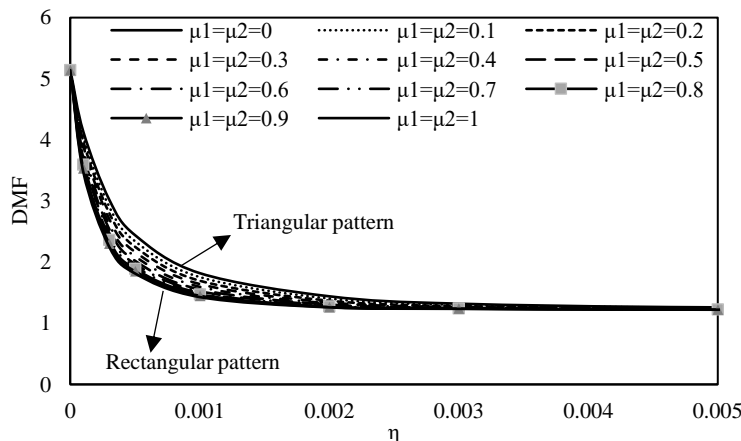


Fig. 10 Dynamic magnification factor (DMF) of tip displacement versus damping parameter  $\eta$  for different shear damping shapes ( $L_d=0.2L$ )

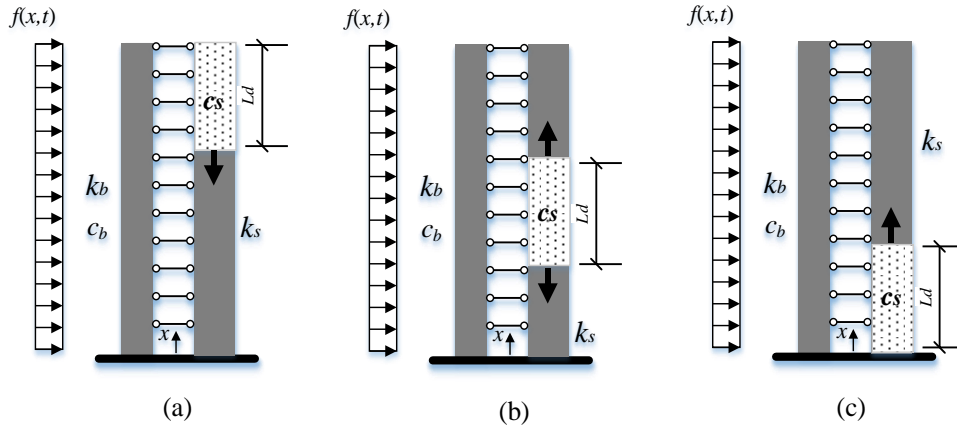


Fig. 11 The CTB system with 5% inherent bending damping  $c_b$  and three arrangements of uniform shear damping  $c_s$  distributed from (a) top (b) maximum rotation position (c) base

now on, the uniform shear damping (i.e.,  $\mu_1=\mu_2=1$ ) is employed in order to analyze the optimal characteristics of damping. Note that the pattern of damping can be the further step after specifying its optimal properties such as the optimum position, amount, and length.

In order to evaluate the efficiency of the proposed strategy related to the optimum placement of damping, a comparative investigation is firstly carried out. For this purpose, a constant shear damping with a fixed amount  $\eta=0.0004$  and the variable length  $L_d$  is considered. Three different locations (i.e., the top, around the peak modal rotation, and the base) are proposed for the initiation of damping (see Fig. 11), respectively, named Arrangement (a), Arrangement (b), and Arrangement (c). The damping model can be distributed downward or upward depending on its initial location. The structure is subjected to the same uniformly harmonic load applied before. To compare the efficiency of aforementioned three arrangements, several responses are plotted in Figs. 12(a)-(d). It can be observed that for all the responses the best efficiency is related to the Arrangement (b), which is based on the shear damping (passive) distributed from the position of maximum rotation. The worst performance belongs to the damping distributed from the base (i.e., Arrangement (c)).

According to the plots shown in Fig. 12, it can be observed that the Arrangement (b) is more efficient than other arrangements even by using a very short damping length (e.g.,  $L_d=0.1L$ ), while Arrangements (a) and (c) give the optimum responses with larger lengths, e.g.,  $L_d=0.65L$  and  $L_d=0.95L$ , respectively, with respect to the DMF response. This means that the application of Arrangement (b) is not only more efficient but also is significantly affordable in comparison with other arrangements. Hence, from now on, the Arrangement (b) is used for the optimization analysis of shear damping in this study.

A sensitivity analysis is also carried out to more confidently demonstrate the superiority of Arrangement (b). Therefore, the same responses shown in Fig. 12 are graphed (see Figs. 13(a)-(d)) against the position of the shear damping  $L_g/x(\vartheta_{max})$ , normalized with respect to the position of maximum rotation  $x(\vartheta_{max})$ . According to the graphs shown in Fig. 13, lengths of the curves are different for each damping value  $\eta$ , because the optimum length of damping associated to each  $\eta$  may be different in the sensitivity analysis. It can be seen from Fig. 13(a) that the forced responses and the optimum values decrease with increasing  $\eta$ . The optimum positions of shear damping are

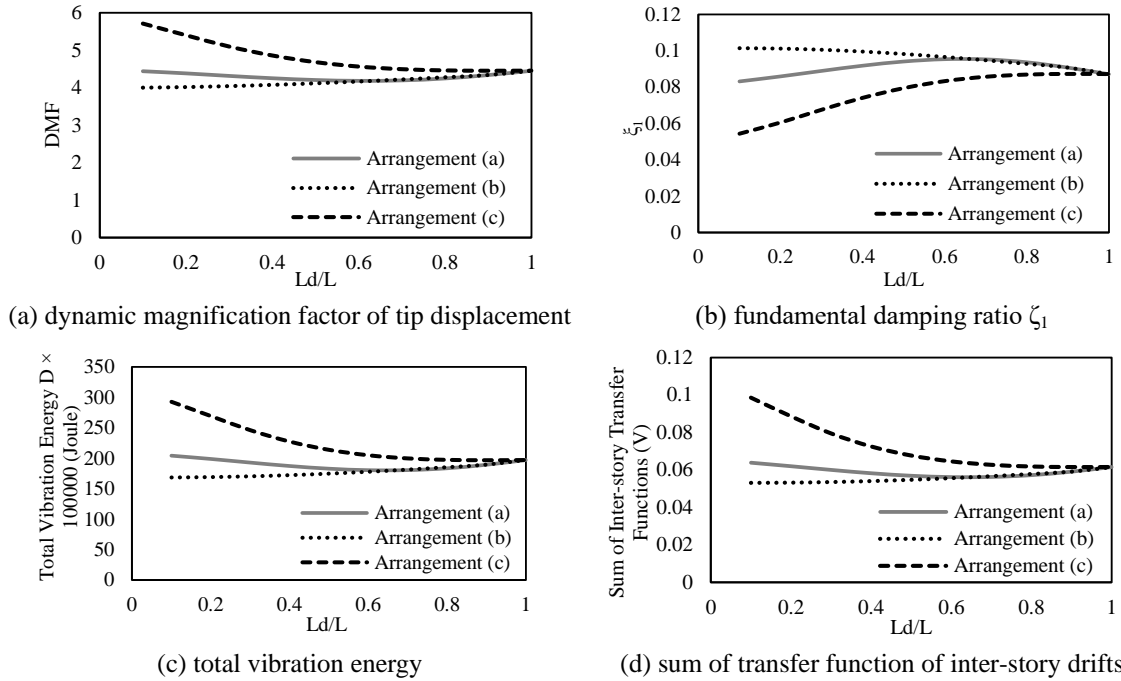
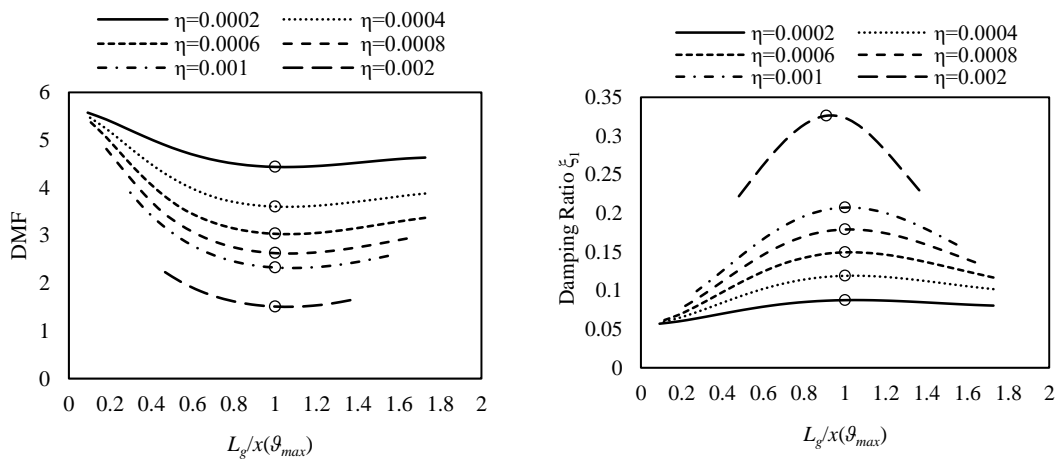


Fig. 12 Evaluation of various responses versus the normalized damping length  $L_d/L$  for three Arrangements (a), (b), and (c)

specified by small circles shown on each curve. Performing the sensitivity analysis, the optimum value of DMF is almost located around  $[L_g/x(\vartheta_{max})]=1$  for every  $\eta$ . In this case, the optimum position of damping can be defined in the range  $1.075 < L_g/x(\vartheta_{max}) < 1.0917$ .



(a) dynamic magnification factor of tip displacement (b) fundamental damping ratio  
 Fig. 13 Sensitivity analysis results versus the normalized position of shear damping with respect to position of maximum modal rotation for different damping parameters  $\eta$

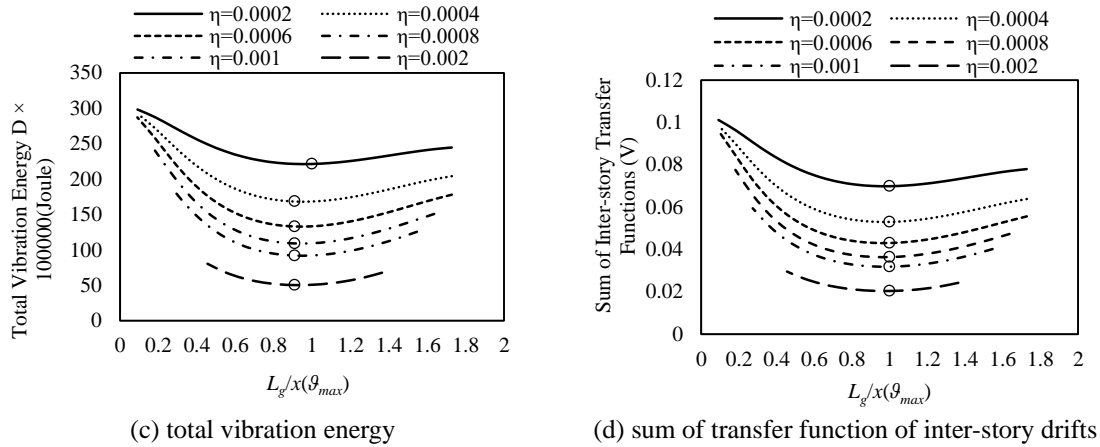


Fig. 13 Continued

The trend of variation in damping ratio  $\zeta_1$  associated to each  $\eta$  (see Fig. 13(b)) shows that the peak ratio is obtained when the center of shear damping is located around the position of maximum rotation. Fig. 13(b) also shows when the shear damping is located far from the position of maximum rotation the level of  $\zeta_1$  decreases, especially when it is closer to the base (i.e.  $[L_g/x(\vartheta_{max})] \ll 1$ ). The positions which are in vicinity of the top (i.e.  $[L_g/x(\vartheta_{max})] \gg 1$ ) are not also prone to obtain the considerable levels of  $\zeta_1$  as those are around the positions of maximum rotation.

Concerning the vibration energy (see Fig. 13(c)), the optimum position of damping varies in the range  $0.91 < L_g/x(\vartheta_{max}) < 1.077$  and is coincided to  $L_g/x(\vartheta_{max}) = 1$  for the sum of transfer function of inter-story drifts (see Fig.13(d)). However, it can be proved that the application of shear damping around the peak modal rotation is reliable in mitigating significantly the vibration and consequently in controlling the responses.

Based on the Arrangement (b), the influence of damping length  $L_d$  with different values of  $\eta$  is investigated on the responses of the reference structure. Therein,  $L_d$  is gradually distributed to affect the whole height. Consequently, the responses are presented in Figs. 14(a)-(d). It can be seen from Fig. 14(a) that, in general, the optimum damping length  $L_d$  associated with the minimum DMF, which are indicated by small circles on each curve, increases with increasing the damping amount  $\eta$ . For instance, for  $\eta=0.0002$  the optimum length is about  $0.1L$  (i.e.,  $L_d=5.6$  m), but it is equal to  $0.3L$  (i.e.,  $L_d=16.8$  m) for  $\eta=0.002$ . It is also obvious that even a small damping length, e.g.,  $L_d=5.6$  m, corresponding to every  $\eta$ , can suppress the dynamic response significantly. This demonstrates once more the dominant efficiency of Arrangement (b) as a proper solution to control dynamic responses.

The overall damping ratios  $\zeta_1$  associated with the fundamental mode, obtained from Eqs. (17)-(23), are graphed in Fig. 14(b). As it is obvious from Fig. 14(b), the minimum damping ratio is the inherent damping  $\zeta_{0,1}=0.05$  corresponding to the 5% of critical bending damping. It can be seen that  $\zeta_1$  increases upon improving the additional damping  $\eta$ , but its increase also depends on the damping length  $L_d$ , showing a specific peak (optimum) value. For example, the maximum damping ratio  $\zeta_1=0.0875$  is identified for  $\eta=0.0002$  with  $L_d=0.1L$ , but  $\zeta_1=0.323$  is achieved for  $\eta=0.002$  where  $L_d=0.5L$  (see Fig. 14(b)).

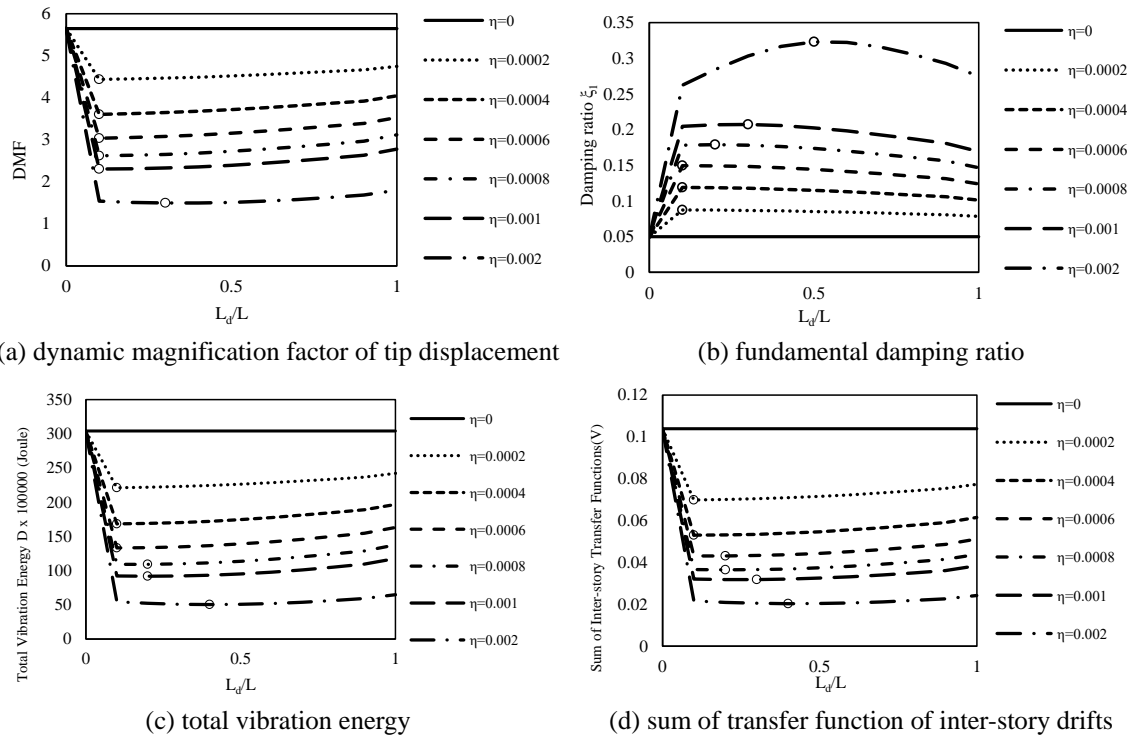


Fig. 14 Trend of various responses versus the normalized damping length  $L_d/L$  for different damping parameters  $\eta$

Figs. 14(c)-(d) indicate, respectively, the total vibrational energy and the sum of transfer functions of inter-story drifts for different values of  $\eta$ . The plots exhibit almost similar trends, as shown in Fig. 14(a) for the DMF of tip displacement, with different optimum lengths  $L_d$ . The efficiency of the proposed strategy is significant, where the shear damping is considerably concentrated (e.g.,  $L_d/L=0.1-0.2$ ) around the location of maximum modal rotation.

With regard to a more general investigation, the variations in DMF of tip displacement and damping ratio  $\zeta_1$  are shown for different degrees of coupling  $\alpha_0^2$  (see Figs. 15(a)-(b)). For this purpose, a uniform shear damping with a fixed amount ( $\eta=0.0002$ ) and length ( $L_d=0.25L$ ) is employed with a variable position  $L_g$  from the base of the CTB. The inherent damping is set to the 5% of bending damping. According to Fig. 15, the optimum locations of additional damping values are found by some small circles. It can be seen from the graphs that the optimum location of damping is lowered with increasing  $\alpha_0^2$ . Moreover, upon improving  $\alpha_0^2$ , the level of DMF and  $\zeta_1$  goes up and down, respectively. It means that, using the shear damping, the systems with smaller  $\alpha_0^2$  are capable of providing greater dissipation mechanism in comparison with those have larger  $\alpha_0^2$ .

#### Optimization of Viscoelastic Dampers

In addition to the viscous dampers modeled using the shear damping, viscoelastic dampers are also analyzed based upon the CTB formulation. To this end, the Viscoelastic Coupling Damper (VCD) developed (Christopoulos and Montgomery 2013) at the University of Toronto is

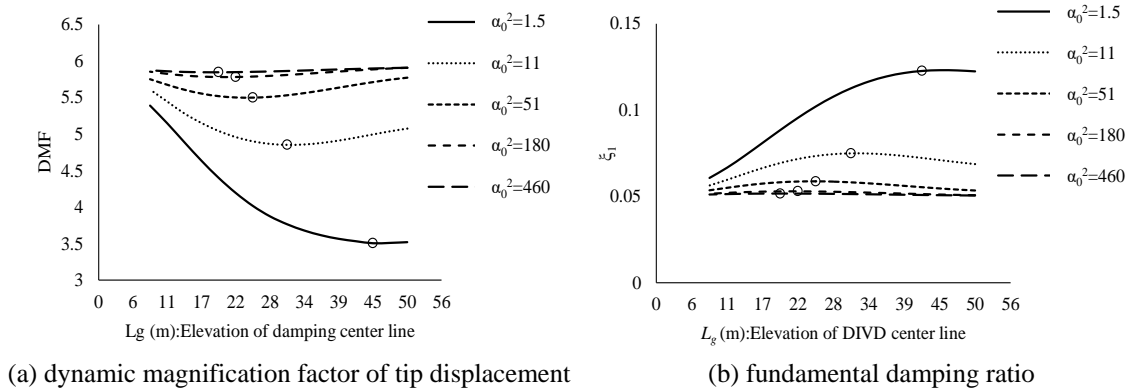


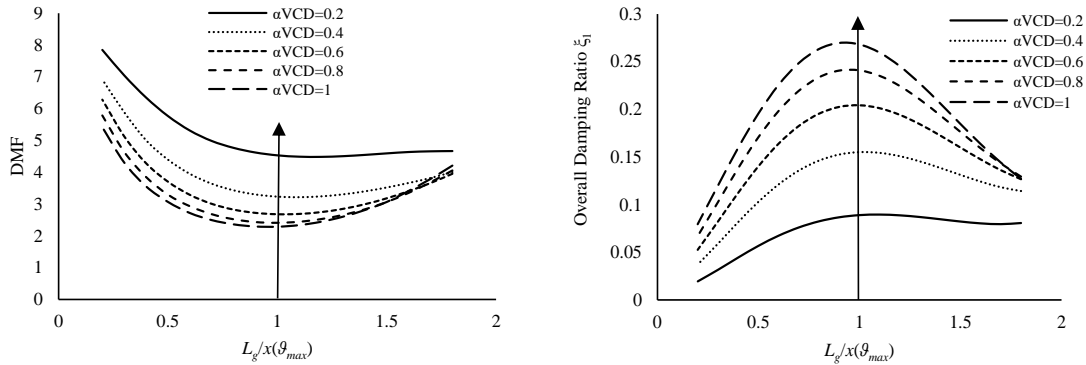
Fig. 15 Sensitivity analysis results versus the position of shear damping for different  $\alpha_0^2$

considered. The VCD can mitigate both wind and earthquake vibrations and achieve significantly more efficient and more resilient high-rise building designs. A simple model used to represent such a damper is illustrated in Fig. 3, which is a spring and a viscous damper in parallel. Despite the fact that during earthquake or wind loading some self-heating is expected in the viscoelastic material as it is strained, it was shown that the viscoelastic material properties are very stable and predictable for the targeted service wind-level and earthquake-level strain amplitudes, frequencies, and loading durations. According to the relevant expression presented in Table 1, to analyze VCD models using the CTB, the distributed equivalent stiffness  $k_{s,eq}$  and damping  $c_s$  associated with a single VCD can be obtained easily.

A designed VCD (Christopoulos and Montgomery 2013) is selected to analyze the reference structure including damping. The viscoelastic material properties used in such a device were based on the expected average properties at the natural period of vibration, a damper material strain of 100% and an average viscoelastic material temperature  $T=24^\circ\text{C}$ . The stiffness and damping coefficients of the VCD in shear were calculated as  $k_{VCD}=162.4 \text{ kN/mm}$  and  $c_{VCD}=134.1 \text{ kN.s/mm}$ , respectively. Note that an additional story mass equal to 500 ton is taken into account to tune the fundamental frequency associated to the dominant mode of the structure as consistent with the vibration frequency in the viscoelastic material. Also, 1 % of bending damping is assigned to the system as the inherent damping. Therein, a controlling parameter  $\alpha_{VCD}$  is considered instead of  $\eta$  in order to simultaneously take into account a wider range of the stiffness and damping properties of VCDs. This parameter may play the role of change in the physical quantities such as the shear area or the ratio between the area and thickness in viscoelastic materials, as the size parameter characteristics.

Accomplishing a sensitivity analysis, the application of shear damping with regard to its location is firstly examined. Hence, a certain number of VCDs, e.g.,  $N_d=4$  (i.e., the length of damped segment equal to  $L_d=11.2$ ) is assumed, and the DMF of tip displacement and damping ratio  $\zeta_1$  are graphed (Figs. 16(a)-(b)) for several values of  $\alpha_{VCD}$  with respect to the normalized position of damping. Similarly to the plots indicated for viscous dampers, it can be found from the latter plots that the strategy proposed based on the position of peak static rotation is yet reliable where viscoelastic materials are used. According to Fig. 16, slight differences are visible which may be due to the addition of VCD stiffness to the system.

Some of those structural indices studied for viscous dampers are plotted (Figs. 17(a)-(c))

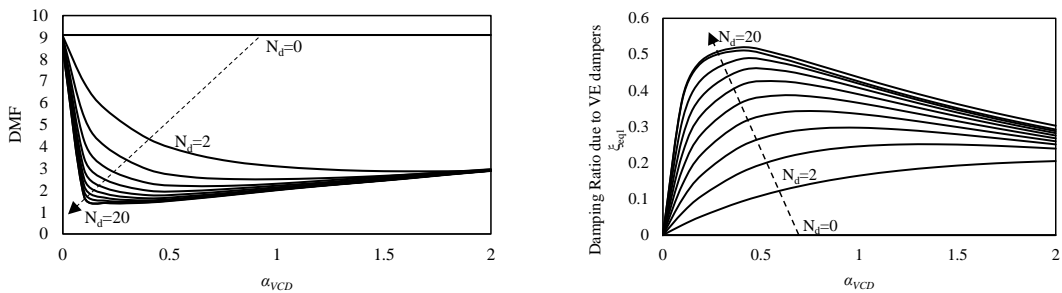


(a) dynamic magnification factor of tip displacement

(b) equivalent damping ratio

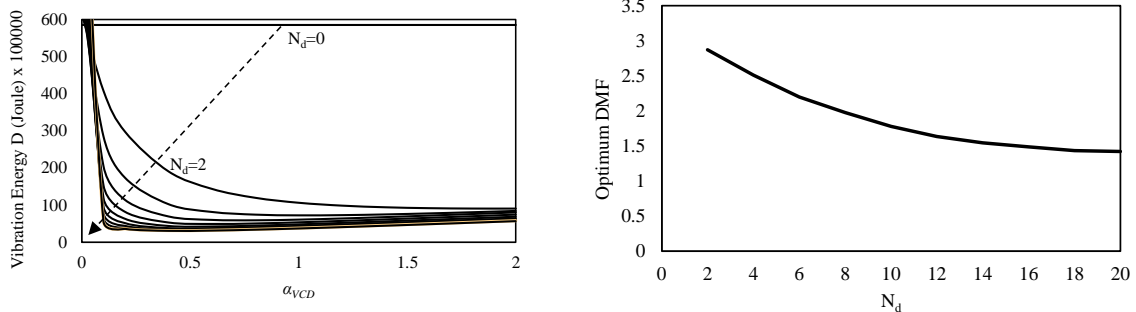
Fig. 16 Sensitivity analysis results versus normalized position of shear damping with respect to position of maximum static rotation for different properties of VCDs

against  $\alpha_{VCD}$  for different numbers  $N_d$  of VCDs. It should be remarked that  $N_d$  is the number of VCDs located around the position of peak static rotation under the uniform static load. It can be observed from Fig. 17(a) that the DMF for every  $N_d$  initially decreases with increasing  $\alpha_{VCD}$  but again increases with passing through a certain value of  $\alpha_{VCD}$ , associated to the minimum DMF. Therefore, the optimum value of  $\alpha_{VCD}$  can be achieved for every number of devices (see Fig.



(a) dynamic magnification factor of tip displacement

(b) equivalent damping ratio  $\zeta_{eq1}$



(c) total vibration energy

(d) optimum dynamic magnification factor

Fig. 17 Trend of dynamical responses versus the viscoelastic property coefficient  $\alpha_{VCD}$  for different number  $N_d$  of VCDs and corresponding optimal curves against  $N_d$

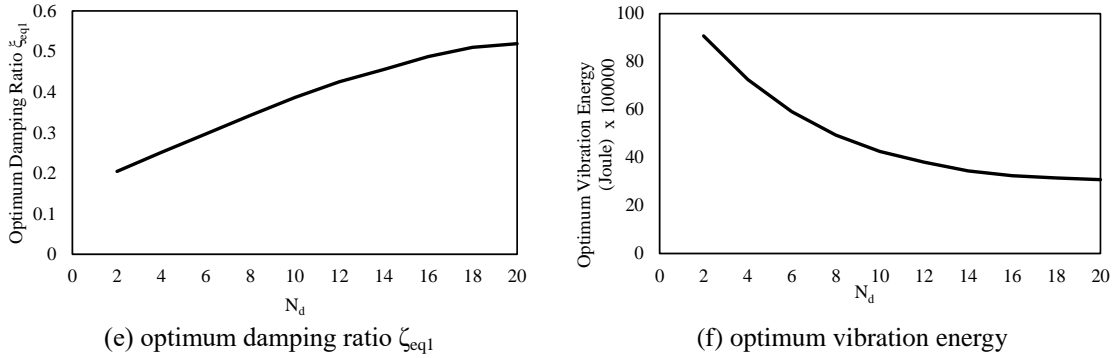


Fig. 17 Continued

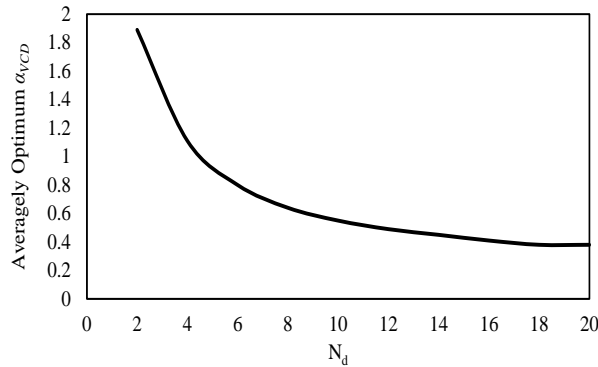


Fig. 18 Average optimum curve of the viscoelastic property against  $N_d$

17(d)). Correspondingly, the trend of damping ratio  $\zeta_1$  (Fig. 17(b)) provided by the VCDs indicates a peak value on each diagram, resulting in a single curve related to the optimum (maximum) damping ratio versus  $N_d$  (see Fig. 17(e)). Concerning the total vibration energy  $D$  (see Fig. 17(c)), in general, a similar trend as resulted for the DMF is found. For small values of  $\alpha_{VCD}$ , a different behavior can be seen in the response, where the diagrams are intersected at given values of  $\alpha_{VCD}$  depending on every  $N_d$ . For example, comparing the diagrams associated to  $N_d=2$  and  $N_d=10$ , a greater vibration energy is generated using 10 VCDs where  $0 < \alpha_{VCD} < 0.0375$ , but less energy is resulted for  $\alpha_{VCD} > 0.0375$  with the same number of devices (i.e.,  $N_d=10$ ) in comparison with the energy under 2 VCDs. The optimum curve associated to the total vibration energy is shown against  $N_d$  in Fig. 17(f). According to all performance indices investigated, an averaged optimum curve is achieved (see Fig. 18) with respect to the number of VCDs located around the position of maximum static rotation.

#### 4. Conclusions

The continuum models can be approximate tools to simply capture some essential dynamic characteristics of ordinary and tall building structural systems. Although these models are usually characterized by proper stiffness parameters; moreover, this study is devoted to generalize them by

introducing appropriate damping mechanisms (bending and shear damping) in addition to the classical viscous damping. This study established that building structural systems might be idealized using a CTB model, where non-classical damping models were accounted for. The application of the CTB in modeling shear wall systems was specifically discussed. Having defined a reference example, it was shown that the bending damping may be more effective dissipation mechanism against the classical one, especially when dealing with higher modes, responses. The shear-type damping is a suitable dissipation mechanism to equivalently model passive dissipating devices with various configurations. Such a damping model is more efficient where the degree of coupling is smaller. A shear damping model distributed non-homogeneously and non-uniformly was proposed, and the damping optimization problems were investigated with respect to the value, the length, and the position. The location of maximum rotation due to the static force and the first rotational mode were suggested as the first optimum estimations of the shear damping position. The numerical investigations and sensitivity analyses established the reliability of these suggestions for both viscous and viscoelastic dampers. This study showed that the application of the continuum-based method including the non-classical damping is simple enough and efficient to model the systems accounting for both inherent and additional damping. The CTB formulations proposed in this paper can be primarily conceived as a first step in dealing with structural engineering problems such as approximate dynamic modeling and pre-design of tall building structural systems.

## References

- Adhikari, S. (2000), "Damping models for structural vibration", Ph.D. Dissertation, Cambridge University, Cambridge.
- Adhikari, S. and Woodhouse, J. (2001), "Identification of damping: Part 1, viscous damping", *J. Sound Vib.*, **243**(1), 43-61.
- Bozdogan, K.B. (2012), "Differential quadrature method for free vibration analysis of coupled shear walls", *Struct. Eng. Mech.*, **41**(1), 67-81.
- Capsoni, A., Vigano, G.M. and Bani-Hani, K. (2013), "On damping effects in Timoshenko beams", *Int. J. Mech. Sci.*, **73**, 27-39.
- Chen, W.R. (2011), "Bending vibration of axially loaded Timoshenko beams with locally distributed kelvin-voigt damping", *J. Sound Vib.*, **330**(13), 3040-3056.
- Christopoulos, C. and Montgomery, M. (2013), "Viscoelastic coupling damper (VCD) for enhanced dynamic performance of high-rise buildings", *Earthq. Eng. Struct. Dyn.*, **12**(15), 2217-2233.
- De Silva, C.W. (2007), *Vibration Damping Control and Design*, CRC Press, Taylor and Francis Group, Boca Raton, Florida, USA.
- Dym, C.L. and Williams H.E. (2007), "Estimating fundamental frequencies of tall buildings", *J. Struct. Eng.*, **135**(9), 1479-1483.
- Faridani, H.M. and Capsoni, A. (2014), "An innovative approach to model dissipation mechanism in coupled shear walls", *Proceedings of the 9th International Conference on Structural Dynamics, EURO-DYN 2014*, Porto, Portugal, June-July.
- Huang, X. and Zhu, H.P. (2013), "Optimal arrangement of viscoelastic dampers for seismic control of adjacent shear-type structures", *Appl. Phys. Eng.*, **14**(1), 47-60.
- Hwang, J.S., Tsai, C.H., Wang, S.J. and Huang, Y.N. (2006), "Experimental study of RC building structures with supplemental viscous dampers and lightly reinforced walls", *Eng. Struct.*, **28**, 1816-1824.
- Hwang, J.S., Huang, Y.N., Yi, S.L. and Ho S.Y. (2008), "Design formulations for supplemental viscous dampers to building structures", *J. Struct. Eng.*, **134**(1), 22-31.

- Kayacık, O., Bruch, J.C., Sloss, J.M., Adali, S. and Sadekm I.S. (2008), "Integral equation approach for piezo patch vibration control of beams with various types of damping", *Comput. Struct.*, **86**(3-5), 357-366.
- Keel, C.J. and Mahmoodi, P. (1986), "Designing of viscoelastic dampers for Columbia Center building", *ASCE, Building Motion in Wind*, Seattle, USA.
- Kocatürk, T. and Şimşek, M. (2006), "Dynamic analysis of eccentrically prestressed viscoelastic Timoshenko beams under a moving harmonic force", *Comput. Struct.*, **84**(31-32), 2113-2127.
- Lavan, O. (2012), "On the efficiency of viscous dampers in reducing various seismic responses of wall structures", *Earthq. Eng. Struct. Dyn.*, **41**(12), 1673-1692.
- Madsen, L., Thambiratnam, D. and Perera, N. (2003), "Seismic response of building structures with dampers in shear walls", *Comput. Struct.*, **81**, 239-253.
- Mahmoodi, P., Robertson, L.E., Yontar, M., Moy, C. and Feld, I. (1987), "Performance of viscoelastic dampers in World Trade Center towers", *Structures Congress on Dynamics of Structures*, Orlando, USA.
- Marko, J., Thambiratnam, D. and Perera, N. (2004), "Influence of damping systems on building structures subject to seismic effects", *Eng. Struct.*, **26**(13), 1939-1956.
- Miranda, E. and Taghavi, S.H. (2005), "Approximate floor acceleration demands in multistory buildings. I: formulation", *J. Struct. Eng.*, **131**(2), 203-211.
- Muravskii, G.B. (2004), "On frequency independent damping", *J. Sound Vib.*, **274**(3-5), 653-668.
- Tsai, T.C., Tsau, J.H. and Chen, C.S. (2009), "Vibration analysis of a beam with partially distributed internal viscous damping", *Int. J. Mech. Sci.*, **51**(11-12), 907-914.
- Potzta, G. and Kollar, L.P. (2003), "Analysis of building structures by replacement sandwich beams", *Int. J. Solid. Struct.*, **40**(3), 535-553.
- Silvestri, S. and Trombetti, T. (2007), "Physical and numerical approaches for the optimal insertion of seismic viscous dampers in shear-type structures", *J. Earthq. Eng.*, **11**(5), 787-828.
- Smith, B.S. and Coull, A. (1991), *Tall Building Structures: Analysis and Design*, John Wiley & Sons, New York, USA.
- Soong, T.T. and Dargush, G.F. (1997), *Passive Energy Dissipation Systems in Structural Engineering*, Wiley Company, New York, USA.
- Sullivan, T.J. and Lago, A. (2010), "Retrofit of RC wall buildings using viscous dampers", *Proceeding of the 14th European Conference on Earthquake Engineering*, Ohrid, Republic of Macedonia.
- Takabatake, H. (2010), "Two-dimensional rod theory for approximate analysis of building structures", *Earthq. Struct.*, **1**(1), 1-19.
- Taghavi, S.H. and Miranda, E. (2005), "Approximate floor acceleration demands in multistory buildings. II: applications", *J. Struct. Eng.*, **131**(2), 212-220.
- Takewaki, I. (2009), *Building Control with Passive Dampers: Optimal Performance-based Design for Earthquakes*, John Wiley & Sons Ltd., Singapore.
- Trombetti, T. and Silvestri, S. (2004), "Added viscous dampers in shear-type structures: the effectiveness of mass proportional damping", *J. Earthq. Eng.*, **8**(2), 275-313.
- Trombetti, T. and Silvestri, S. (2006), "On the modal damping ratios of shear-type structures equipped with Rayleigh damping systems", *J. Sound Vib.*, **292**, 21-58.
- Tarjan, G. and Kollar, L.P. (2004), "Approximate analysis of building structures with identical stories subjected to earthquake", *Int. J. Solid. Struct.*, **41**(5), 1411-1433.
- Zalka, K.A. (2001), "A simplified method for calculation of the natural frequencies of wall-frame buildings", *Eng. Struct.*, **23**(12), 1544-1555.
- Zalka, A.K. (2012), *Structural Analysis of Regular Multi-Storey Buildings*, CRC Press, Taylor & Francis Group, Boca Raton, Florida, USA.
- Zarubinskaya, M.A. and Van Horssen, W.T. (2005), "On an improved elastic dissipation model for a cantilevered beam", *Quart. Appl. Math.*, **63**(4), 681-690.